The Astrophysical Journal Letters, 792:L21 (5pp), 2014 September 1 doi:10.1088/2041-8205/792/1/L21

MULTI-WAVELENGTH AFTERGLOWS OF FAST RADIO BURSTS

Shuang-Xi Yi[1,2], He Gao[2], and Bing Zhang[2]
[1] School of Astronomy and Space Science, Nanjing University, Nanjing 210093, China
[2] Department of Physics and Astronomy, University of Nevada, Las Vegas, NV 89154, USA; zhang@physics.unlv.edu
Received 2014 July 1; accepted 2014 July 31; published 2014 August 20

ABSTRACT

The physical origin of fast radio bursts (FRBs) is unknown. Detecting electromagnetic counterparts to FRBs in other wavelengths is essential to measure their distances and to determine their physical origin. Assuming that at least some of them are of cosmological origin, we calculate their afterglow light curves in multiple wavelengths (X-rays, optical, and radio) by assuming a range of total kinetic energies and redshifts. We focus on forward shock emission, but also consider the possibility that some of the FRBs might have bright reverse shock emission. In general, FRB afterglows are too faint to be detected by current detectors. Only if an FRB has a very low radiative efficiency in radio (hence, a very large kinetic energy), and when it is close enough to observe can its afterglow be detected in the optical and radio bands. We discuss observational strategies for detecting these faint afterglows using future telescopes such as Large Synoptic Survey Telescope and Expanded Very Large Array.

Key words: gamma-ray burst: general – radiation mechanisms: non-thermal

Online-only material: color figures

1. INTRODUCTION

Fast radio bursts (FRBs) are mysterious transients that have been discovered recently (Lorimer et al. 2007; Thornton et al. 2013). Their physical origin is subject to intense debate (e.g., Falcke & Rezzolla 2014; Totani 2013; Kashiyama et al. 2013; Popov & Postnov 2013; Zhang 2014; Loeb et al. 2014; Kulkarni et al. 2014). If at least some FRBs are of cosmological origin, as indicated by their anomalously large dispersion measure (DM), their redshift information together with their measured DM offer powerful tools for studying their cosmology, including inferring the baryon content and reionization history of the universe (Deng & Zhang 2014; Kulkarni et al. 2014) and directly constraining cosmological parameters and the dark matter equation of state (Gao et al. 2014; Zhou et al. 2014).

The error boxes of FRBs detected by the Parkes multi-beam survey are typically hundreds of square arcminutes (Thornton et al. 2013). It is therefore difficult to pin down their host galaxies and derive their redshifts. Detecting counterparts of FRBs in other wavelengths is essential for localizing FRBs. Kashiyama et al. (2013) suggested binary white dwarf mergers as the source of FRBs and proposed possible associations of some FRBs with Type Ia supernovae or X-ray debris disk emission. Motivated by *Swift* data showing evidence of a supra-massive neutron star collapsing into a black hole (Troja et al. 2007; Lyons et al. 2010; Rowlinson et al. 2010, 2013; Lü & Zhang 2014; Yi et al. 2014), Zhang (2014) suggested the possible association of a small fraction of FRBs with gamma-ray bursts (GRBs). Two tentative associations of FRB-like events with GRBs may have been discovered by Bannister et al. (2012).[3] Unfortunately, the redshifts of the two GRBs were not measured.

Another possible method of searching for FRB counterparts is to search for their afterglows. Zhang (2014) estimated the brightness of FRB afterglows and found that it is very faint owing to their low energy. He suggested that for a typical FRB at a cosmological distance, the peak radio afterglow flux is dimmer than the FRB itself by 6–7 orders of magnitude (at the μJy level). In this Letter, we calculate the multi-wavelength FRB afterglows in detail.

[3] A negative search result was reported by Palaniswamy et al. (2014), but the time windows of some of these GRBs did not cover the end of the plateau, which is the expected epoch of FRB emission (Zhang 2014).

2. THE MODEL

We apply the standard external shock synchrotron emission afterglow model of GRBs (Mészáros & Rees 1997; Sari et al. 1998; see Gao et al. 2013b for a recent, detailed review). The simplest afterglow model has several free parameters: the total kinetic energy E, the initial Lorentz factor η, the number density of the ambient medium n_0, the equipartition parameters ε_e and ε_B for electrons and magnetic fields, respectively, and the electron injection spectral index p. If one considers a pair of (forward and reverse) shocks, the micro-physics parameters can be different for the two shocks, so altogether one has nine parameters.

The forward shock (FS) emission component is guaranteed. Whether or not a bright reverse shock (RS) emission component exists depends on the unknown magnetization parameter (the ratio between the Poynting flux and the matter flux, usually denoted as σ) of the outflow (Zhang & Kobayashi 2005; Mimica et al. 2009; Mizuno et al. 2009). Most FRB models invoke highly magnetized neutron stars or black holes (e.g., Falcke & Rezzola 2014; Totani 2013; Zhang 2014; Popov & Postnov 2013). For example, in the "magnetic hair" ejection model invoking the implosion of a supra-massive neutron star (Falcke & Rezzola 2014; Zhang 2014), an FRB is emitted in the ejected magnetosphere. The outflow is therefore likely highly magnetized at the central engine. The outflow is accelerated via a magnetic pressure gradient (e.g., Komissarov et al. 2009; Granot et al. 2011) so that σ decreases with radius with the expense of increasing Γ. Significant magnetic dissipation would also occur during the FRB emission phase. Therefore, the σ value after the dissipation, especially at the deceleration radius, is not known. If it is already below unity, as envisaged in some models (e.g., Zhang & Yan 2011), a bright RS emission component may be expected (Zhang et al. 2003; Zhang & Kobayashi 2005).

In the following, we neglect these complications and only consider a standard fireball defined by the total energy E and initial Lorentz factor η. For faint afterglows of FRBs, to the first

order the details of jet composition would not affect the global picture.

The deceleration timescale $t_\times$, which is also the time when the RS crosses the shell (for a non-magnetized outflow), can be approximated as

$$t_\times \sim \frac{l(1+z)}{2c\eta^{8/3}}, \quad (1)$$

where $l = (3E/4\pi n_0 m_p c^2)^{1/3}$ is the Sedov length.

Both E and η are poorly constrained. The observed FRBs have an energy of $E_{\rm FRB} \sim 10^{38}$–10^{40} erg assuming a redshift of $z \sim (0.5$–$1)$ (Thornton et al. 2013). Observations of radio pulsars suggest that their radio emission efficiency is typically low, especially for more energetic ones (Szary et al. 2014). As a result, the total kinetic energy in an FRB outflow can be significantly greater than the FRB energy. Within the supra-massive neutron star implosion scenario, the total energy in the ejecta is essentially the total magnetic energy of the neutron star magnetosphere, which can be as large as $\sim 10^{47}$ erg for a magnetar (Zhang 2014). In the following, we allow E to be in a wide range from 10^{43} to 10^{47} erg.

Various constraints on the FRB emission mechanisms suggest that the bulk motion Lorentz factor of an FRB is at least 100 (e.g., Falcke & Rezzolla 2014; Katz 2014). In the following, we adopt a conservative value $\eta = 100$. At $t \gg t_\times$, the predictions of afterglow flux do not depend on η. For a higher η, $t_\times$ would move to an earlier epoch and the peak afterglow flux would be increased accordingly. For $E = 10^{47}$ erg, $\eta = 100$, and $n_0 \sim 1{\rm cm}^{-3}$, one has $t_\times \sim 3$ s.

The synchrotron radiation spectrum from the FS or RS can be characterized by a multi-segment broken power law separated by three characteristic frequencies: the minimum synchrotron frequency (corresponding to electrons with the minimum Lorentz factor), the cooling frequency ν_c, and the self-absorption frequency ν_a (Sari et al. 1998). The peak flux of the spectrum is denoted as $F_{\nu,\rm max}$. Based on the standard prescription (e.g., Sari et al. 1998; Wu et al. 2003; Yi et al. 2013; Gao et al. 2013b), one can calculate the afterglow emission from FRBs. At the shock crossing time $t_\times$, the FS emission can be characterized by

$$\nu^f_{\rm m,\times} = 4.1\times10^{16}\,\varepsilon^{1/2}_{B,f,-2}\,\varepsilon^{2}_{e,-1}\,n_0^{1/2}\,\eta_2^4\,(1+z)^{-1}\,{\rm Hz}, \quad (2)$$

$$\nu^f_{c,\times} = 7.5\times10^{19}\,\varepsilon^{-3/2}_{B,f,-2}\,n_0^{-5/6}\,\eta_2^{4/3}\,E_{47}^{-2/3}(1+z)^{-1}\,{\rm Hz}, \quad (3)$$

$$\nu^f_{a,\times} = 7.4\times10^{8}\,\varepsilon^{1/5}_{B,f,-2}\,\varepsilon^{-1}_{e,-1}\,n_0^{3/5}\,E_{47}^{1/5}\,(1+z)^{-1}\,{\rm Hz}, \quad (4)$$

$$F^f_{\nu,\rm max,\times} = 7.8\times10^{-6}\,\varepsilon^{1/2}_{B,f,-2}\,n_0^{1/2}\,E_{47}\,D_{L,27}^{-2}\,(1+z)\,{\rm Jy}. \quad (5)$$

Here the typical shock micro-physics parameters are normalized to $\varepsilon_e = 0.1$, $\varepsilon_B = 0.01$, and $p = 2.5$. The evolution of the four parameters (Mészáros & Rees 1997; Sari et al. 1998; Yi et al. 2013; Gao et al. 2013b)

$$t < t_\times:\ \nu^f_a \propto t^{\frac{3}{5}},\ \nu^f_m \propto t^0,\ \nu^f_c \propto t^{-2},\ F^f_{\nu,\rm max} \propto t^3, \quad (6)$$

and

$$t > t_\times:\ \nu^f_a \propto t^0,\ \nu^f_m \propto t^{-\frac{3}{2}},\ \nu^f_c \propto t^{-\frac{1}{2}},\ F^f_{\nu,\rm max} \propto t^0. \quad (7)$$

Because of its low total energy, an FRB outflow would reach the non-relativistic phase in a relatively short period of time. The transition time is when the bulk Lorentz factor $\gamma - 1 = 1$, where $\gamma \sim (3E/32\pi n_0 m_p c^5 t^3)^{1/8}$. After this transition time, the scaling law of the FS emission is modified as

$$\nu^f_a \propto t^{\frac{6}{5}},\quad \nu^f_m \propto t^{-3},\quad \nu^f_c \propto t^{-\frac{1}{5}},\quad F^f_{\nu,\rm max} \propto t^{\frac{3}{5}}. \quad (8)$$

The non-relativistic phase transition time is roughly $t_{\rm N} \sim 6.6\times10^4, 1.4\times10^4, 3.1\times10^3$ s for with $E = 10^{47}, 10^{45}, 10^{43}$ erg, respectively.

If a putative RS exists, the four parameters (ν_m, ν_c, ν_a, $F_{\nu,\rm max}$) of the two shocks can be related to each other at $t_\times$, which depend on the ratios between the micro-physics parameters of the two shocks (Kobayashi & Zhang 2003; Zhang et al. 2003). When explicitly written, these four parameters are

$$\nu^r_{m,\times} = 1.3\times10^{13}\varepsilon^{1/2}_{B,r,-1}\,\varepsilon^{2}_{e,-1}n_0^{1/2}\eta_2^2(1+z)^{-1}\,{\rm Hz}, \quad (9)$$

$$\nu^r_{c,\times} = 2.4\times10^{18}\varepsilon^{-3/2}_{B,r,-1}n_0^{-5/6}\eta_2^{4/3}E_{47}^{-2/3}(1+z)^{-1}\,{\rm Hz}, \quad (10)$$

$$\nu^{\rm r}_{a,\times} = 7.2\times10^{11}\,\varepsilon^{1/5}_{B,r,-1}\,\varepsilon^{-1}_{e,-1}\,n_0^{3/5}\,\eta_2^{8/5}\,E_{47}^{1/5}(1+z)^{-1}{\rm Hz}, \quad (11)$$

$$F^r_{\nu,\rm max,\times} = 2.5\times10^{-3}\,\varepsilon^{1/2}_{B,r,-1}n_0^{1/2}\eta_2 E_{47}D_{L,27}^{-2}(1+z)\,{\rm Jy}. \quad (12)$$

Note that ε_B is normalized to 0.1 since the outflow is likely magnetized.

The scaling laws of RS before and after the crossing time are (e.g., Kobayashi 2000; Yi et al. 2013; Gao et al. 2013b)

$$t < t_\times:\ \nu^r_a \propto t^{-\frac{33}{10}},\ \nu^r_m \propto t^6,\ \nu^r_c \propto t^{-2},\ F^r_{\nu,\rm max} \propto t^{\frac{3}{2}}, \quad (13)$$

and

$$t > t_\times:\ \nu^r_a \propto t^{-\frac{102}{175}},\ \nu^r_m \propto t^{-\frac{54}{35}},\ \nu^r_c \propto t^{-\frac{54}{35}},\ F^r_{\nu,\rm max} \propto t^{-\frac{34}{35}}. \quad (14)$$

3. RESULTS

Figure 1 shows the calculated FS FRB afterglow light curves in the X-ray (2 keV, panel (a)), optical (R-band, panel (b)), and radio (1 GHz, panel (c)) bands, respectively. Three different energies, i.e., $E = 10^{47}$ erg (blue), 10^{45} erg (red), and 10^{43} erg (green), and three different redshifts, i.e., $z = 0.5$ (dashed), 0.1 (dash-dotted), and 0.01 (solid), have been adopted. Other parameters are fixed to the typical values: $\eta = 100, n_0 = 1{\rm cm}^{-3}$, $p = 2.5$, $\epsilon_{B,f} = 0.01$, and $\epsilon_e = 0.1$. The sensitivity lines of different detectors in different energy bands are also plotted. The black solid line in panel (a) is the sensitivity line of the *Swift*/X-Ray Telescope (XRT), which is $\propto t^{-1}$ early on and breaks to $\propto t^{-1/2}$ when $F_\nu = 2.0\times10^{-15}{\rm erg\,cm^{-2}\,s^{-1}}$ at $t = 10^5$ s (Moretti et al. 2009; D. N. Burrows 2014, private communication). The black solid line in panel (b) is the sensitivity line of the Large Synoptic Survey Telescope (LSST) Array. In the survey mode, LSST reaches 24.5 mag in 30 s (R. Margutti 2014, private communication). The black solid line in panel (c) is the sensitivity line of the Expanded Very Large Array (EVLA),[4] which scales as $\propto t^{-1/2}$ for arbitrarily long exposure times.

In general, the broad-band FRB afterglows are all very faint except in cases of a large E and a small z, when the predicted afterglow flux becomes of an observational interest. As shown in

[4] The Exposure Calculator can be found at https://obs.vla.nrao.edu/ect/.

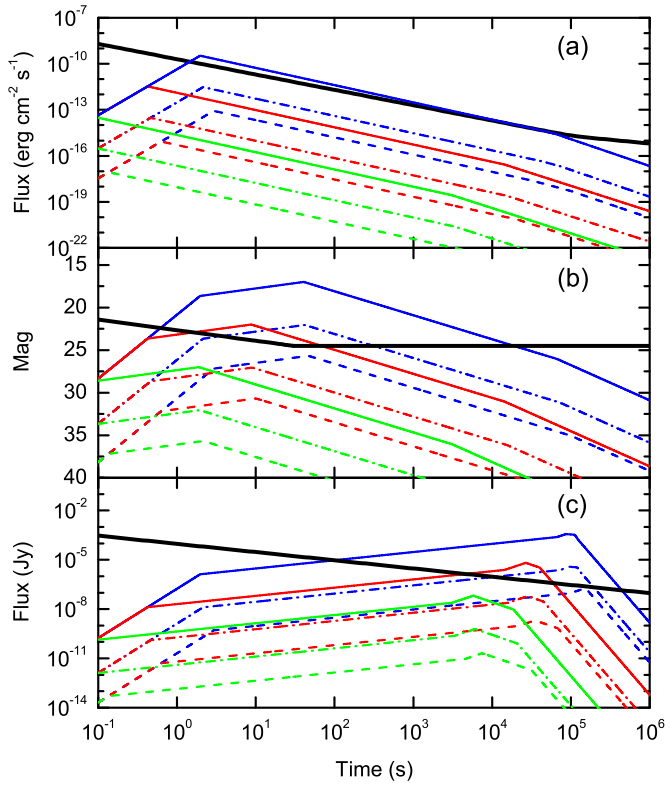

Figure 1. Example forward shock afterglow light curves of FRBs. The model parameters: $\epsilon_B = 0.01$, $\epsilon_e = 0.1$, $n_0 = 1$, $p = 2.5$, and $\eta = 100$. Three values of the energy $E = 10^{47}$ (blue), 10^{45} (red), 10^{43} (green), and three values of redshift $z = 0.5$ (dashed), 0.1 (dash-dotted), 0.01 (solid) have been adopted. (a) The X-ray light curves at 2 keV. The black solid line is the detector sensitivity line of *Swift*/XRT. (b) *R*-band light curves. The black solid line is the detector sensitivity line of LSST. (c) Radio light curves at 1 GHz. The black solid line is the detector sensitivity line of EVLA.

(A color version of this figure is available in the online journal.)

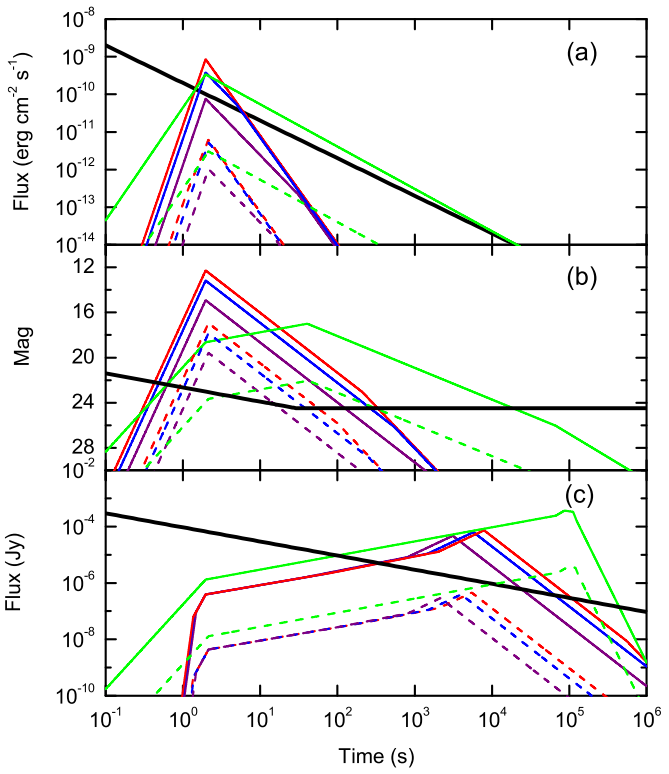

Figure 2. Example reverse shock afterglow light curves of FRBs. The model parameters: $\epsilon_e = 0.1$, $n_0 = 1$, $p = 2.5$, and $\eta = 100$. Only the most optimistic cases with energy $E = 10^{47}$ and redshift $z = 0.01$ (solid) and $z = 0.1$ (dashed) are plotted. Several $R_{\rm B}$ values are adopted to calculate the RS component: $R_{\rm B} = 2$ (purple), 5 (blue), and 8 (red). The FS component is shown as green in both cases, and the black solid lines are the detector sensitivity lines (same as Figure 1). (a) The X-ray light curves at 2 keV. (b) *R*-band light curves. (c) Radio light curves at 1 GHz.

(A color version of this figure is available in the online journal.)

Figure 1, the X-ray afterglow becomes detectable by *Swift*/XRT only for the most optimistic case calculated, i.e., $E = 10^{47}$ erg, and $z = 0.01$ (panel (a)). In the optical *R* band (panel (b)), the peak magnitude of the FS light curves is about 17, 22, and 26, respectively, for $z = 0.01, 0.1, 0.5$ and $E = 10^{47}$ erg. The LSST may catch the peak emission only when $z < 0.2$ for $E = 10^{47}$ erg. In the 1 GHz radio band (panel (c)), the peak flux density is about 4.4×10^{-4} Jy, 4.2×10^{-6} Jy, and 1.5×10^{-7} Jy, respectively, for $z = 0.01, 0.1, 0.5$ and $E = 10^{47}$ erg. This would be detected by EVLA only when $z < 0.2$ for $E = 10^{47}$ erg. The peak time shifts to later times with decreasing frequency. This suggests that follow-up observations are easier in low frequencies. For example, with $E = 10^{47}$ erg, the peak time in 1 GHz is around 1 day.

We also consider the RS emission from FRBs in Figure 2. Fixing other parameters, we allow $\varepsilon_{B,r}$ to be higher than $\varepsilon_{B,f}$ assuming that the outflow is likely highly magnetized. Defining $R_{\rm B} = (\varepsilon_{B,r}/\varepsilon_{B,f})^{1/2}$ (Zhang et al. 2003), we calculate the cases for $R_{\rm B} = 2$ (purple), 5 (blue), and 8 (red). We fix $E = 10^{47}$ erg and consider $z = 0.01$ and $z = 0.1$, with the FS emission (green) plotted as a reference. One can see that with a large $R_{\rm B}$, the RS component would outshine the FS component, especially in the optical and radio bands, making it easier to detect. The afterglow is detectable by LSST and EVLA at $z < 0.2$.

To better display how peak time and peak flux depend on E and z, in Figure 3 we show the contours of peak time and peak flux in the $E-z$ space. The three panels are for X-rays (panel (a)), optical (panel (b)), and radio (panel (c)), respectively. The X-ray peak time is simply the deceleration time $t_\times$. For the optical band, the peak time is defined when ν_m crosses the band. For the radio band, the peak time is defined when $\max(\nu_m, \nu_a)$ crosses the band. For the peak flux, we present two (FS versus RS) values, with the RS value presented in parentheses (noting the same E- and z-dependences of $F^f_{\nu,\rm max}$ and $F^r_{\nu,\rm max}$. Since the sensitivity of LSST in the survey mode is a constant (24.5 mag), we also plotted two thick lines (24.5 mag) above which LSST can detect the FS (magenta) and RS (green) emissions, respectively.

Assuming that most observed FRBs are at $z \sim 1$, one can derive the event rate for FRBs below a certain redshift. Assuming that the total event rate density is a constant, i.e., $\rho \sim 10^{-3}$ gal^{-1} yr^{-1} (Thornton et al. 2013), a smaller redshift corresponds to a small volume, and hence, a small event rate. Taking an event rate of $\sim 10^4$ sky^{-1} day^{-1} at $z \sim 1$ (Thornton et al. 2013), one can draw the expected event rate as a function of z based on volume correction. This is shown as blue dotted lines in the three contour plots. Note that the event rate is subject to large uncertainties. For example, recently, Petroff et al. (2014) reported a lack of FRBs at intermediate Galactic latitudes, which suggests either a possible anisotropy of FRB distribution or a lower event rate. Our event rate curve is still relevant as long as one re-normalizes the $z = 1$ event rate to the value determined by future observations.

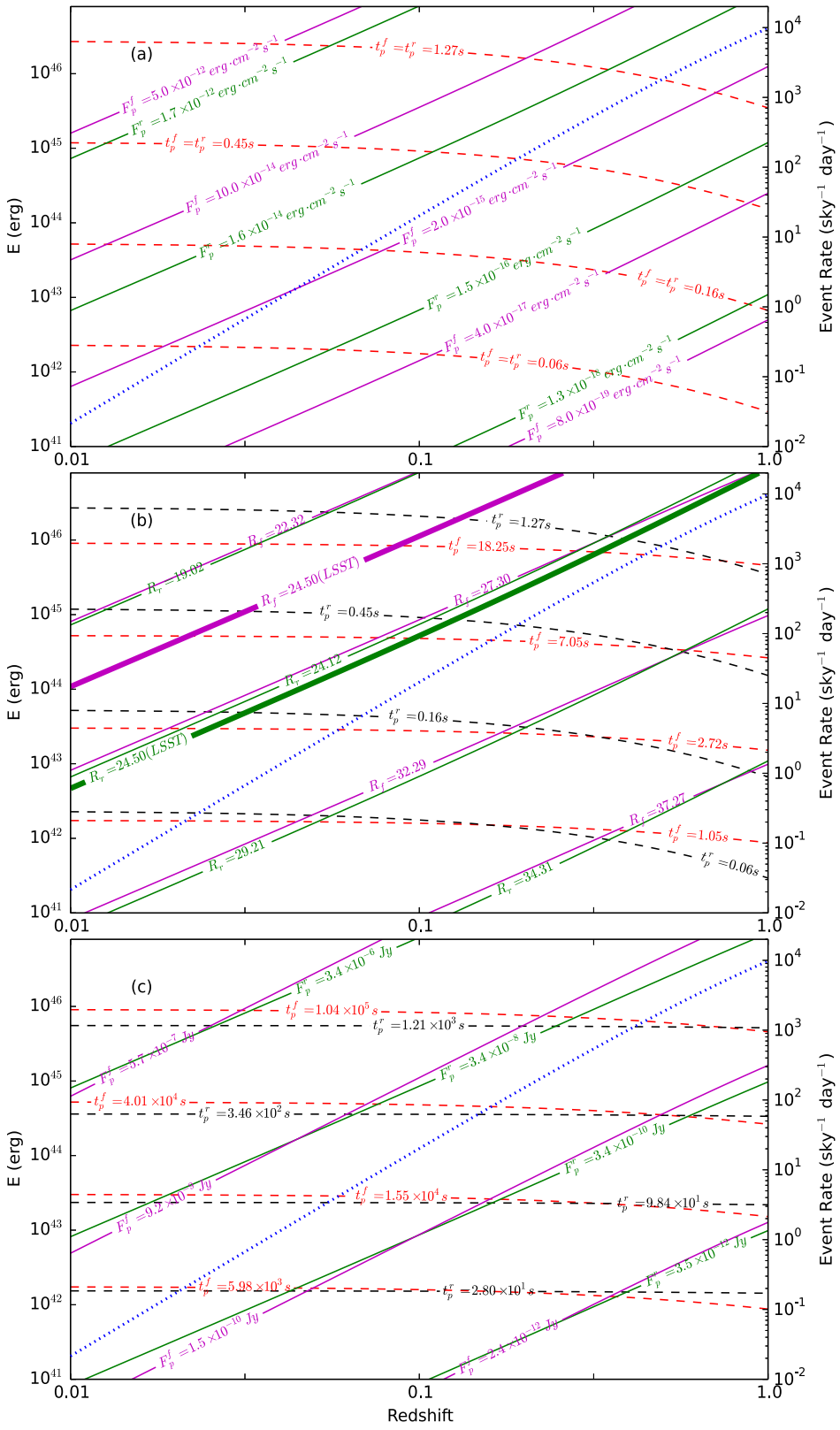

Figure 3. Contours of peak time and peak flux in the $E-z$ plane. The peak times are marked with dashed lines (the red for FS and the black for RS), and peak fluxes are marked with solid lines (the purple for FS and the green for RS). The blue dotted line in each panel denotes the detection event rate (right vertical label). Panels (a), (b), and (c) are for X-rays, optical, and radio bands, respectively. Thick lines in panel (b) are the sensitivity lines of LSST in the survey mode: FS (magenta) and RS (green).

(A color version of this figure is available in the online journal.)

4. SUMMARY AND DISCUSSION

In this Letter, we apply the standard GRB afterglow model to predict possible afterglow emission from FRBs. We calculate their afterglow light curves in X-rays, optical, and radio by assuming a range of their total kinetic energies and redshifts. In general, owing to their low energies, the broad-band afterglow emission is predicted to be very faint, especially for the FS only. Only if the total kinetic energy of FRBs is very large (radio efficiency very low), and in rare cases when some of them are close enough to Earth, could their FS afterglows become (barely) detectable by the current instruments. It is unclear whether there is a bright RS component from FRBs. If so (which requires significant de-magnetization before deceleration), the chance of detecting FRB afterglow in the optical and radio bands is higher, although still challenging.

Since data analyses needed to claim the detection of an FRB take significant time, and since the X-ray afterglow of an FRB peaks early and decays rapidly, follow-up observations of FRBs with XRTs (e.g., *Swift*/XRT) would not be fruitful. A better strategy for detecting an X-ray counterpart of an FRB is to apply a wide-field XRT (such as the Einstein Probe or Lobster), which may catch an X-ray transient associated with an FRB. However, such a telescope is still being proposed, and it is believed that several other types of X-ray transients, e.g., supernova shock breakouts (Soderberg et al. 2008), jets from tidal disruption events (Burrows et al. 2011; Bloom et al. 2011), and putative X-ray transients due to neutron star–neutron star mergers with a millisecond magnetar engine (Zhang 2013; Gao et al. 2013a; Yu et al. 2013; Metzger & Piro 2014),[5] would give rise to brighter X-ray signals than the FRB afterglow. Detecting X-ray transients associated with FRBs is plausible, but challenging.

In the optical band, the FS peak time is after $t_\times$, while the RS peak time is at $t_\times$. Again, due to the possible delay in the data analysis required to claim an FRB discovery, follow-up observations may not be fruitful. One should also appeal to wide-field optical telescopes, such as GWAC (Paul et al. 2011). The peak flux is, however, usually too low to be detected by these telescopes unless the source is energetic, nearby, and has a bright RS emission component. The optical afterglow peak emission can be detected by LSST for nearby energetic events in the survey mode. However, since only 7–10 square degrees are covered in each 30 s exposure (E. Berger 2014, private communication), it still takes a great chance coincidence to detect the optical afterglow of an FRB with LSST.

In the radio band, the telescope that detects the FRB can continue to collect data. As a result, no trigger information is needed to "follow up" an FRB. On the other hand, the afterglow is faint. For a Jy level FRB, the peak afterglow flux is in the μJy level for the FS component for typical parameters, and at most, one order of magnitude brighter for the RS component. For optimistic cases (large E and small z), the afterglow flux may reach the mJy level, but the detection rate for these extreme cases is very low. In general, large radio telescopes with high sensitivity are needed. In principle, one can use a small radio telescope to trigger an FRB and use a large telescope to follow up. The peak time of radio afterglow is 10^4–10^6 s (hours to days). This would be a good strategy if the data processing time to claim an FRB detection can be reduced to within hours. Follow-up observations with EVLA would be able to catch the FRB afterglow if the source is energetic and nearby.

The afterglow emission signal discussed in this Letter is *generic* to progenitor models. It is also the *minimum* multi-wavelength signal one would expect to be associated with an FRB. Subject to progenitor models, an FRB may be accompanied by other, brighter signals (e.g., Kashiyama et al. 2013; Zhang 2014; Niino et al. 2014), which can be used to differentiate among the progenitor models.

We thank Edo Berger, David Burrows, and Raffaella Margutti for helpful discussions on the instrumental sensitivities of EVLA, LSST, and *Swift* XRT. This research was partially supported by the National Basic Research Program (973 Program) of China (grant No. 2014CB845800).

[5] Double neutron star mergers can leave behind a supra-massive rapidly spinning neutron star if the masses of the two neutron stars are small and the neutron star equation of state is hard (Dai et al. 2006; Gao & Fan 2006).

REFERENCES

Bannister, K. W., Murphy, T., Gaensler, B. M., & Reynolds, J. E. 2012, ApJ, 757, 38
Bloom, J. S., Giannios, D., Metzger, B. D., et al. 2011, Sci, 333, 203
Burrows, D. N., Frank, K. A., & Park, S. 2014, BAAS, 223, 353.14
Burrows, D. N., Kennea, J. A., Ghisellini, G., et al. 2011, Natur, 476, 421
Dai, Z. G., Wang, X. Y., Wu, X. F., & Zhang, B. 2006, Sci, 311, 1127
Deng, W., & Zhang, B. 2014, ApJL, 783, L35
Falcke, H., & Rezzolla, L. 2014, A&A, 562, A137
Gao, H., Ding, X., Wu, X.-F., Zhang, B., & Dai, Z.-G. 2013a, ApJ, 771, 86
Gao, H., Lei, W.-H., Zou, Y.-C., Wu, X.-F., & Zhang, B. 2013b, NewARv, 57, 141
Gao, H., Li, Z., & Zhang, B. 2014, ApJ, 788, 189
Gao, W.-H., & Fan, Y.-Z. 2006, ChJAA, 6, 513
Granot, J., Komissarov, S. S., & Spitkovsky, A. 2011, MNRAS, 411, 1323
Kashiyama, K., Ioka, K., & Mészáros, P. 2013, ApJL, 776, L39
Katz, J. I. 2014, PhRvD, 89, 103009
Kobayashi, S. 2000, ApJ, 545, 807
Kobayashi, S., & Zhang, B. 2003, ApJL, 582, L75
Komissarov, S. S., Vlahakis, N., Königl, A., & Barkov, M. V. 2009, MNRAS, 394, 1182
Kulkarni, S. R., Ofek, E. O., Neill, J. D., Zheng, Z., & Juric, M. 2014, arXiv:1402.4766
Loeb, A., Shvartzvald, Y., & Maoz, D. 2014, MNRAS, 439, L46
Lorimer, D. R., Bailes, M., McLaughlin, M. A., Narkevic, D. J., & Crawford, F. 2007, Sci, 318, 777
Lü, H.-J., & Zhang, B. 2014, ApJ, 785, 74
Lyons, N., O'Brien, P. T., Zhang, B., et al. 2010, MNRAS, 402, 705
Mészáros, P., & Rees, M. J. 1997, ApJ, 476, 232
Metzger, B. D., & Piro, A. L. 2014, MNRAS, 439, 3916
Mimica, P., Giannios, D., & Aloy, M. A. 2009, A&A, 494, 879
Mizuno, Y., Zhang, B., Giacomazzo, B., et al. 2009, ApJL, 690, L47
Moretti, A., Pagani, C., Cusumano, G., et al. 2009, A&A, 493, 501
Niino, Y., Totani, T., & Okumura, J. E. 2014, PASJ, submitted (arXiv:1407.1088)
Palaniswamy, D., Wayth, R. B., Trott, C. M., et al. 2014, ApJ, 790, 63
Paul, J., Wei, J., Basa, S., & Zhang, S.-N. 2011, CRPhy, 12, 298
Petroff, E., van Straten, W., Johnston, S., et al. 2014, ApJL, 789, L26
Popov, S. B., & Postnov, K. A. 2013, arXiv:1307.4924
Rowlinson, A., O'Brien, P. T., Metzger, B. D., Tanvir, N. R., & Levan, A. J. 2013, MNRAS, 430, 1061
Rowlinson, A., O'Brien, P. T., Tanvir, N. R., et al. 2010, MNRAS, 409, 531
Sari, R., Piran, T., & Narayan, R. 1998, ApJL, 497, L17
Soderberg, A. M., Berger, E., Page, K. L., et al. 2008, Natur, 453, 469
Szary, A., Zhang, B., Melikidze, G. I., Gil, J., & Xu, R.-X. 2014, ApJ, 784, 59
Thornton, D., Stappers, B., Bailes, M., et al. 2013, Sci, 341, 53
Totani, T. 2013, PASJ, 65, L12
Troja, E., Cusumano, G., O'Brien, P. T., et al. 2007, ApJ, 665, 599
Wu, X. F., Dai, Z. G., Huang, Y. F., & Lu, T. 2003, MNRAS, 342, 1131
Yi, S.-X., Dai, Z.-G., Wu, X.-F., & Wang, F. Y. 2014, arXiv:1401.1601
Yi, S.-X., Wu, X.-F., & Dai, Z.-G. 2013, ApJ, 776, 120
Yu, Y.-W., Zhang, B., & Gao, H. 2013, ApJL, 776, L40
Zhang, B. 2013, ApJL, 763, L22
Zhang, B. 2014, ApJL, 780, L21
Zhang, B., & Kobayashi, S. 2005, ApJ, 628, 315
Zhang, B., Kobayashi, S., & Mészáros, P. 2003, ApJ, 595, 950
Zhang, B., & Yan, H. 2011, ApJ, 726, 90
Zhou, B., Li, X., Wang, T., Fan, Y.-Z., & Wei, D.-M. 2014, PhRvD, 89, 107303